Banding in Simple Steady Shear of Entangled Polymer Solutions

Sham Ravindranath, Shi-Qing Wang,* Michael Olechnowicz, and Roderic P. Quirk

Department of Polymer Science and Maurice Morton, Institute of Polymer Science, University of Akron, Akron, Ohio 44325-3909

Received December 7, 2007; Revised Manuscript Received January 27, 2008

ABSTRACT: Velocity profiles of six entangled polybutadiene solutions (PBD) have been determined during startup shear using a particle tracking velocimetric (PTV) technique, where the number Z of entanglements per chain in these solutions varies from 13 to 119, depending on the PBD molecular weight and solution concentration. Flow behavior of these solutions at various rates in the stress plateau region has been investigated in both parallel-disk and cone−plate cells. For the least entangled solution with $Z = 13$, homogeneous shear was observed under all flow conditions. The solution with $Z = 27$ displayed inhomogeneous shear after the stress maximum before returning to a linear velocity profile at long times. For solutions with $Z \geq 40$, shear banding was observed in both transient and steady states for a range of shear rates in the stress plateau region. At sufficiently high rates, shear homogeneity returns in steady state for these solutions ($Z \geq 40$) after initial banding.

1. Introduction

Entangled polymer melts and solutions undergo various flows before ending up in final products. Accurate understanding of nonlinear flow behavior of entangled polymers will be helpful in optimizing processing and in achieving desirable properties through processing. Cone−plate, planar Couette, and circular Couette shear cells, presumably capable of producing uniform shear rate across the gap, have been widely used to generate startup shear,[1–12] and interpretation of rheometric measurements is conventionally made with the assumption of homogeneous shear. A central aim in polymer rheology was to obtain constitutive relation, the simplest of which is true steady-state shear stress as a function of applied shear rate. Most existing studies reported a monotonic relation between stress and shear rate[3,6,9–12] and produced an impression that there was no shear banding for well-entangled polymers, although it is unclear whether steady-state measurements have ever been attained in these studies.

Assuming that entangled wormlike micelles would behave like entangled polymer chains, micellar solutions had been regarded for a long time as the only polymer like system to possess true stress plateau.[13,14] Such a feature encouraged experimental efforts to look for and discover shear banding in wormlike entangled micellar solutions.[15–24] The observed shear inhomogeneity is plausible due to the character that the "polymer chains" are living; i.e., the chain connectivity is achieved through noncovalent bonding and may be readily breakable in flow. Because of this possibility, we did not previously think that shear banding in wormlike micellar solutions necessarily implies occurrence of inhomogeneous shear in entangled polymer solutions. This partially explains the 10 year gap between the first report of shear banding in entangled micellar solutions[15] and that in entangled polymer solutions.[25,26] Although many theoretical studies of shear banding at a continuum level using constitutive models[27–29] were inspired by the experimental studies of micellar solutions, they did not lead to an examination of whether and why shear banding should be observable in entangled polymer solutions and melts.

A modern theoretical description of startup shear of entangled polymers is mostly based on Doi–Edwards (DE) tube model.[30] In absence of any experimental suggestion of a nonmonotonic constitutive curve, the original DE tube theory has been rectified to produce a monotonic constitutive relation using the concepts of convective constraint release and contour length fluctuations.[31–34] After the first report of shear banding across sample thickness in an entangled polybutadiene solution,[25,26] there was a constant speculation that this newly revealed character is consistent with the prediction of the original Doi–Edwards theory that anticipated a nonmonotonic relation between shear stress and shear rate.[35] However, a subsequent study revealed macroscopic motions during relaxation after cessation of a large step shear,[36,37] in contrast to the theoretical perception of the original DE theory that only quiescent molecular diffusion would be possible after step strain. Thus, it has become doubtful whether or not a proper theoretical account of shear banding could emerge from the DE theory.

Table 1. Molecular Characteristics of Long Chain 1,4-Polybutadienes

sample	M_n (g/mol)	M_w (g/mol)	M_w/M_n	source	1,4%/1,2% addition	1,4-cis/ 1,4-trans
0.7M	0.74×10^6	0.75×10^6	1.02	Bridgestone	92/8	56/36
1M	1.01×10^6	1.05×10^6	1.03	Akron	96/4	68/28
1.8M	1.56×10^6	1.86×10^6	1.19	Goodyear	92/8	56/36

Previous experimental observations[25,26] of shear banding highlight the inability of entangled fluids to maintain uniform deformation when sheared on time scales faster than the terminal relaxation time. A notable shortcoming of the previous studies is that the entangled fluid was sheared only for a small amount of strain units and "steady-state" velocity profiles at various applied shear rates were unknown. Using circular Couette shear cell, Hu et al.[38] attempted to determine steady-state velocity profiles in such entangled solutions and concluded that no shear banding would be expected in steady state for entangled polymers.

The present work is carried out to provide an extensive quantification of transient and steady-state velocity profiles of a number of entangled solutions with the number Z of entanglements per chain ranging from 13 to 119 since the previous PTV studies did not address the issue of how the level of chain entanglement would influence the shear banding characteristics. Velocity profiles both in parallel-disk and cone−plate shear cells have been examined for a range of shear rates in the stress plateau region. The present work contains mainly PTV data from the parallel-disk cell and only chooses one solution of $Z = 64$ to show PTV results from both shear cells.

* Corresponding author. E-mail: swang@uakron.edu.

10.1021/ma7027352 CCC: $40.75
Published on Web 03/08/2008

Table 2. Molecular Characteristics of Various Solvents at Room Temperature

sample	M_n (g/mol)	M_w (g/mol)	source	η_s (Pa·s)	1,4%/1,2% addition	1,4-cis/ 1,4-trans
PBD-2K	1800		Sigma-Aldrich Cat. No. 20,043-3 (60% unsaturation, phenyl terminated)	97	15/45	5/10
PBD-9K	8500	8900	Goodyear	10	92/8	56/36
PBD-15K	14000	15000	Bridgestone	36	92/8	56/36

Table 3. Molecular Characteristics of Entangled PBD Solutions at Room Temperature

sample	Z	$M_e(\phi)$ (kg/mol)	τ (s)	η (Pa·s)
0.7M (5%)-2K	13	57	40	21062
0.7M (10%)-9K	27	27	16	56911
1M (10%)-9K	40	26	63	2.3×10^5
1M (15%)-9K	64	16	65	5.1×10^5
1.8M (10%)-9K	70	26	71	
1.8M (15%)-15K	119	15	250	

2. Experimental Section

2.1. Materials. The present PTV study is based on six entangled 1,4-polybutadiene (PBD) solutions. The molecular characteristics of three parent PBD used to make entangled solutions are listed in Table 1. The PBD sample labeled as 0.7M was provided through courtesy of C. Robertson at Bridgestone-America, 1M PBD was made at University of Akron, and 1.8M PBD was provided through courtesy of A. Halasa at Goodyear. The entangled solutions were prepared using oligomeric butadiene solvents whose molecular characteristics are listed in Table 2. Various polymeric "solvents" were chosen to suppress interfacial wall slip.[37] This strategy to suppress interfacial slip works because previous work has shown[39] that the viscosity η and terminal relaxation time τ of a binary polymer mixture hardly scales linearly with the "solvent" viscosity η_s. Thus, the slip length, which is related to the viscosity ratio η/η_s, can be greatly reduced by employing a polymeric solvent of sufficiently high molecular weight and corresponding high value of η_s.

These solutions were prepared by first dissolving high-molecular-weight PBD in toluene to which oligomeric butadiene was added. Silver-coated silica particles with an average diameter of 10 μm (Danted Dynamics HGS-10), first ultrasonicated in toluene, was added to the polymeric solution such that the final loading of the particles was 200–600 ppm. Most of the toluene was evaporated slowly under a hood for days, and the remaining was removed in vacuum conditions until the residue is less than 0.5%. Since T_g of 1,4-PBD is ca. −100 °C, any residual toluene of this level is not rheologically noticeable and thus of no consequence. The molecular characteristics and linear viscoelastic properties of all the entangled solutions are briefly summarized in Table 3, where the number of entanglements per chain, $Z = (M_w/M_e)\phi^{1.2}$, with M_w being the molecular weight of the parent PBD, M_e the entanglement molecular weight for PBD melts taken to be 1600 g/mol, and ϕ being polymer weight fraction. From oscillatory shear measurements at room temperature, the terminal relaxation time τ and zero-shear viscosity η can be determined, except for the polydisperse solution. 0.7M (5%)-2K solution refers to 5 wt % of 0.7M PBD (listed in Table 1) dissolved in 95 wt % of 2K oligomeric butadiene (listed in Table 2). The rest of the samples are also labeled in the same manner.

2.2. Apparatuses. To determine the linear viscoelastic properties of the six entangled solutions, small-amplitude oscillatory-shear (SAOS) frequency sweep measurements were conducted using an Advanced Rheometrics Expansion System (ARES) at room temperature. All startup shear experiments in controlled-rate mode were carried out with a Bohlin-CVOR rheometer at room temperature, except for one ARES-based experiment involving the 1M (10%)-9K solution at shear rate of 0.09 s^{-1}. For the 5 and 10 wt % solutions, measurements were made on a 35 mm diameter parallel-disk cell, and for the two 15 wt % solutions a 25 mm diameter parallel disk was employed to stay within the torque limit of the rheometer. The flow profiles of 1M (15%)-9K solution having $Z = 64$ was also analyzed using cone−plate geometry of $\theta = 5.4°$ and diameter 25 mm. Focusing on determination of velocity profiles with PTV setup and being less accurate in the rheological measurements, the meniscus was wrapped with a thin flexible film to prevent sample loss.

2.3. Particle Tracking Velocimetry (PTV) Setup. The PTV setup has been described elsewhere.[37] For solutions with concentrations of 5% and 10%, a 35 mm diameter parallel-disk cell was used where PTV observations were made at a radial distance of 8 mm from the meniscus. For the solutions of concentration 15%, velocity profile determination was made at a radial distance of 4 mm from the meniscus for either a 25 mm diameter parallel-disk cell or a 25 mm diameter cone−plate cell. In the case of parallel-disk measurements, the average shear rate refers to the location of the PTV observation plane. All measurements were carried out at room temperature around 25 °C. It is worth mentioning that the current PTV setup has an inherent error of ca. 15% in its reading of the sample gap that produces the same level of uncertainty in the determination of velocity profiles. However, such a small imperfection has little consequences since the revealed shear inhomogeneity is typically rather severe.

3. Results and Discussion

3.1. Homogeneous Shear. Flow behavior of the least entangled solution 0.7M (5%)-2K with $Z = 13$ is investigated first in 35 mm parallel-disk on a Bohlin-CVOR rheometer. The chain dynamics of this solution was made sluggish by using high vinyl (45%) phenyl terminated oligomeric BD as the solvent. Figure 1a shows small-amplitude oscillatory-shear (SAOS) frequency sweep measurements, indicating a terminal relaxation time of $\tau = 40$ s for the long chains in the sluggish solvent. The sluggish dynamics makes the entire stress plateau accessible rheologically and resolvable by our PTV measurements. Figure 1b shows the velocity profile of the sample at a radial distance of 8 mm from the edge according to our PTV observations. It is noted that one of the rates, 0.25 s^{-1} presented in Figure 1b, is in the middle of the stress plateau, while the other, 3.5 s^{-1}, is at the end of the plateau. For the two rates, velocity profiles before the shear stress overshoot and after the overshoot and in steady state are presented in Figure 1b. From Figure 1b, it can be seen that the velocity profiles hardly deviate from linearity; i.e., the sample experiences uniform shear at all times. Apparently, at such a low level of entanglement, the solution is not sufficiently solidlike to respond inhomogeneously upon a suddenly applied external deformation at a rate faster than the terminal relaxation time. Observations were similar for other shear rates in the stress plateau regime and in cone−plate geometry.

3.2. Transient Shear Banding. The second entangled solution 0.7M (10%)-9K based on the same parent polymer 0.7M PBD but with a higher concentration of 10 wt % has $Z = 27$. Linear viscoelastic properties of this solution are shown in Figure 2a. To probe the nonlinear region of this solution, the shear rates at PTV observation plane are chosen to be faster than the overall chain relaxation rate. Figures 2b and c show the velocity profiles at different instants for local shear rates of 1, 2, and 3 s^{-1} as observed at a radial distance of 8 mm from the edge. Stress growth at rates 1 and 3 s^{-1} are plotted in the inset of Figures 2b and c, respectively, where the vertical arrows indicate the times when the velocity profiles are determined. As seen in Figure 2b, the velocity profile is homogeneous at

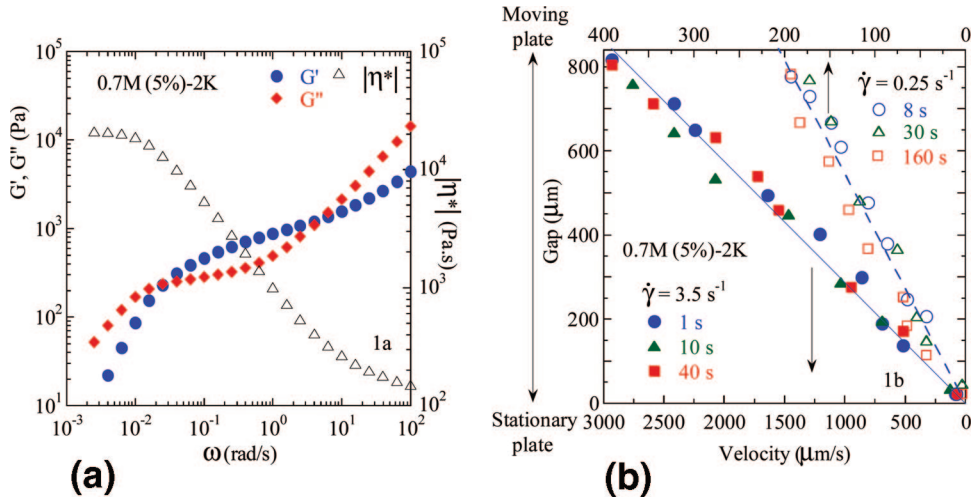

Figure 1. (a) Dynamic storage modulus G', loss modulus G'', and complex viscosity $|\eta^*|$ of 0.7M (5%)-2K solution from oscillatory shear measurements using a strain amplitude of 2% at room temperature. The measurements were made on an ARES rheometer. (b) Particle-tracking velocimetric (PTV) measurements of the velocity profiles at different times. A 35 mm parallel-disk cell was used on a Bohlin-CVOR rheometer.

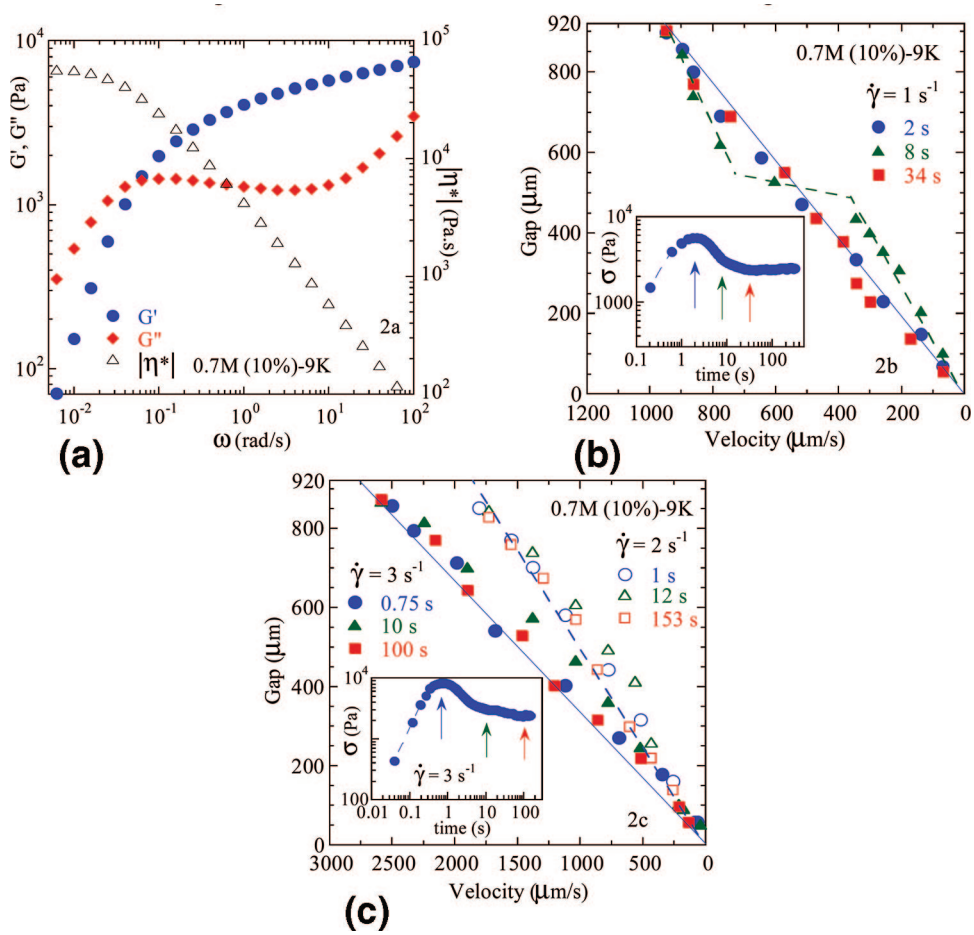

Figure 2. (a) Linear viscoelastic measurements of 0.7M (10%)-9K solution at room temperature. (b) Particle-tracking velocimetric (PTV) measurements of the velocity profiles at different times. A 35 mm parallel-disk cell was employed on Bohlin-CVOR rheometer. The inset shows the corresponding shear stress vs time data and arrows in the inset indicate the times where the profiles were determined. (c) Velocity profiles of 3 and 2 s^{-1} at different times, and the inset shows the rheological data of 3 s^{-1}. Arrows indicating the locations where flow profiles were obtained.

2 s but exhibits nonlinearity at 8 s after shear stress overshoot and returns to a completely linear profile in steady state at 34 s. Similar trends can be seen from Figure 2c for rates of 2 and 3 s^{-1}. With linear velocity profile in steady state, the sample can be viewed to undergo shear thinning homogeneously across the gap. Thus, for modestly entangled polymers, it is feasible for conventional rheological characterization to provide reliable information about their constitutive behavior. For rates outside the range of 0.5−4 s^{-1}, transient shear banding was observed to be progressively weaker. Similar flow behavior has been found when 9K oligomeric BD was replaced by a 2K or 3K oligomeric BD.

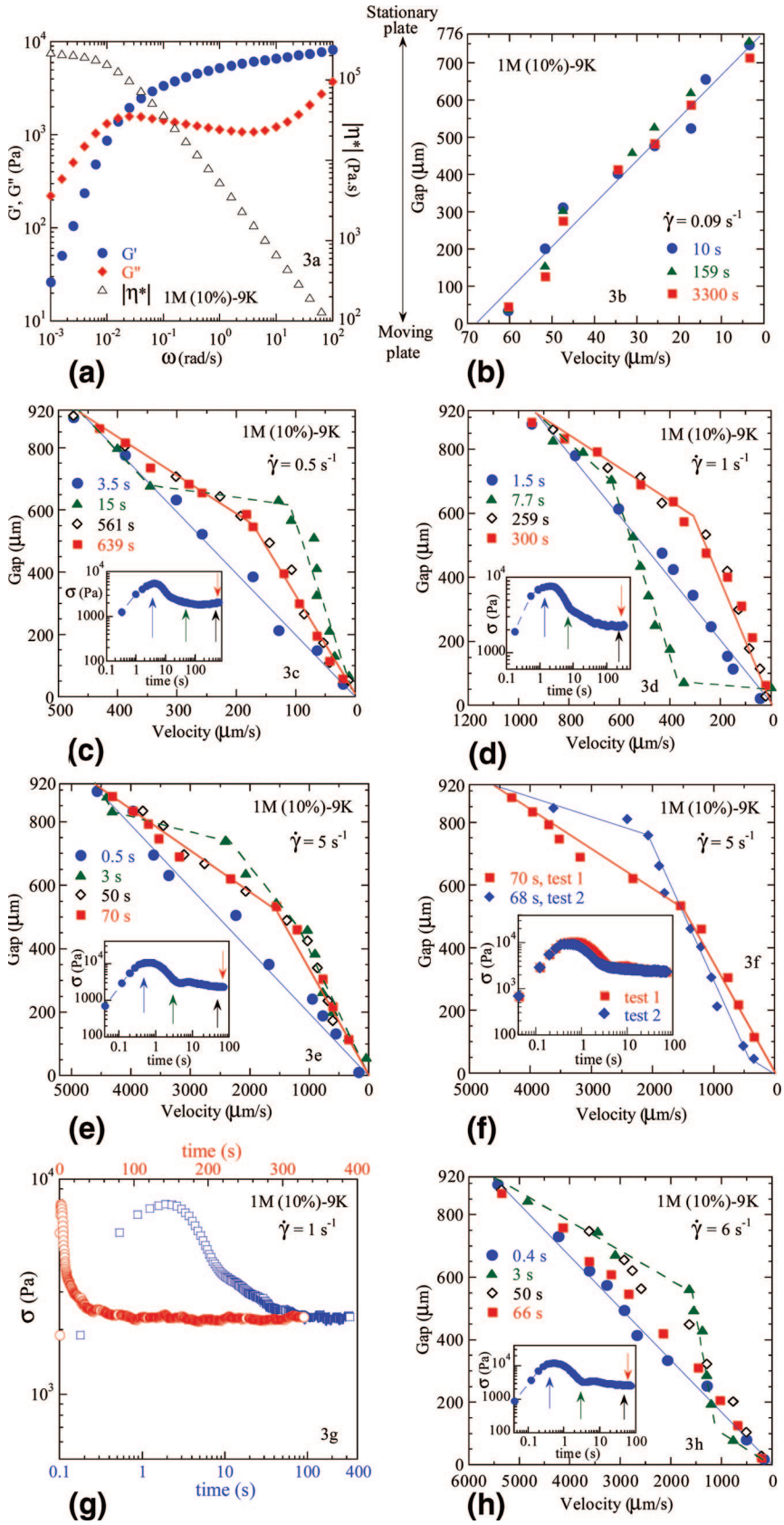

Figure 3. (a) Linear viscoelastic measurements of 1M (10%)-9K solution at room temperature. (b) Velocity profiles of 0.09 s^{-1} at different times measured on ARES rheometer using 35 mm parallel disk where, in contrast to Bohlin, the bottom surface rotates with the top staying fixed. (c−e) Velocity profiles at different times for shear rates mentioned in the figures. Corresponding rheological data have been shown in the inset. A 35 mm parallel-disk cell were employed on a Bohlin-CVOR rheometer. (f) Two different steady-state velocity profiles at the same applied rate of 5 s^{-1}, where the inset shows corresponding stresses as a function of time. A 35 mm parallel-disk cell was employed on a Bohlin-CVOR rheometer. (g) Shear stress data plotted as a function of time on either a linear or logarithmic scale in the case of (d) where the apparent shear rate is 1 s^{-1}. (h) Restoration of near-linear velocity profile at a sufficiently high applied rate.

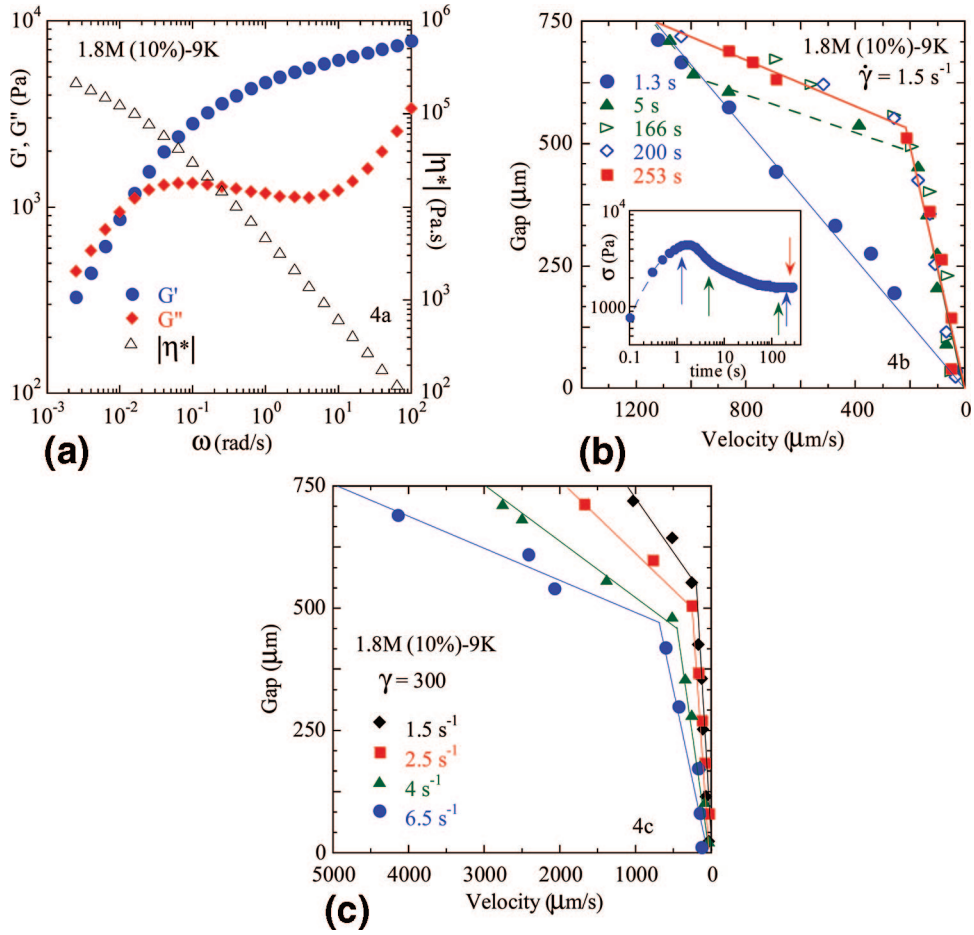

Figure 4. (a) Linear viscoelastic measurements of 1.8M (10%)-9K solution at room temperature. (b) Velocity profiles of 1.5 s^{-1} at different times measured on a Bohlin rheometer using a 35 mm parallel disk. (c) Velocity profiles at 300 strain units are summarized for the various rates mentioned in the figure.

3.3. Steady-State Shear Banding and Restoration of Uniform Shear. *A. 1M (10%)-9K, Z = 40.* To probe the flow behavior of a more entangled system, a third solution, 1M (10%)-9K of $Z = 40$, was studied. Linear viscoelastic properties at room temperature are described in Figure 3a, which reveals a terminal relaxation time of $\tau = 63$ s. As with the previous two solutions, a 35 mm parallel-disk cell was used to make PTV measurements, and the location of observation plane was 8 mm from the edge. Transient and steady-state velocity profiles at various shear rates in the stress plateau region are shown in Figures 3b–f. The profiles just before stress overshoot, immediately after the overshoot, and in steady state are represented respectively by closed circles, closed triangles, and closed squares. Open diamonds show lack of change at long times and suggest attainment of steady state represented by the squares.

First, for a shear rate of 0.09 s^{-1}, i.e., at a Weissenberg number of $0.09 \times 63 = 5.7$, transient and steady-state velocity profiles are essentially linear at all times, as shown in Figure 3b. Figures 3c−f show the velocity profiles at shear rates that are well inside the stress plateau. For all the shear rates indicated in Figure 3c−e, it can be observed that the flow profile represented by the closed circles just before the stress overshoot is homogeneous, and after the overshoot a highly nonlinear profile develops as shown by the closed triangles in the plots. From Figure 3c−e, it can be observed that for various rates the location of the fault plane is different. It is also important to mention that the location where the high-shear region emerged in the gap is different for a given rate among the different repeats. Figure 3f shows this contrast of different velocity profiles corresponding to the same applied rate, measured from two separate loadings of the same sample.

After the initial severe banding, the sample adjusts its velocity profile over many strain units to settle down to a steady state, represented by closed squares in Figure 3c−e when the shear stress also assumes a steady value. Here, the data are plotted against the logarithmic time in order to display the characteristic stress overshoot. Such a presentation also greatly compressed the data at long times, making the attainment of steady stress less visually impressive. On a linear scale, the data can be seen to remain constant at long times as shown in Figure 3g for the case of shear rate equal to 1 s^{-1}. It is obvious from Figure 3c−f that shear inhomogeneity persists even after several hundreds of strain units, and the sample essentially divides itself into high-shear and low-shear regions. Comparison between open diamonds and closed squares indicates that in steady state the velocity profile hardly varies.

According to an emerging picture proposed recently, external deformation implemented at sufficiently high rates can cause a well-entangled polymer (that is an elastic solid on short time scales due to chain entanglement) to undergo cohesive structural breakup.[40] The inhomogeneously disintegrated "solid" is the starting point for the subsequent flow. Naturally, the flow after the yield point could be inhomogeneous. Indeed, the present study confirms several previous reports[25,26,38] that transient shear banding takes place in well-entangled polymer solutions due to the sudden startup shear. What is surprising is that the initial shear inhomogeneity does not adjust back to a state of uniformity even after hundreds of strain units. There appears to be some

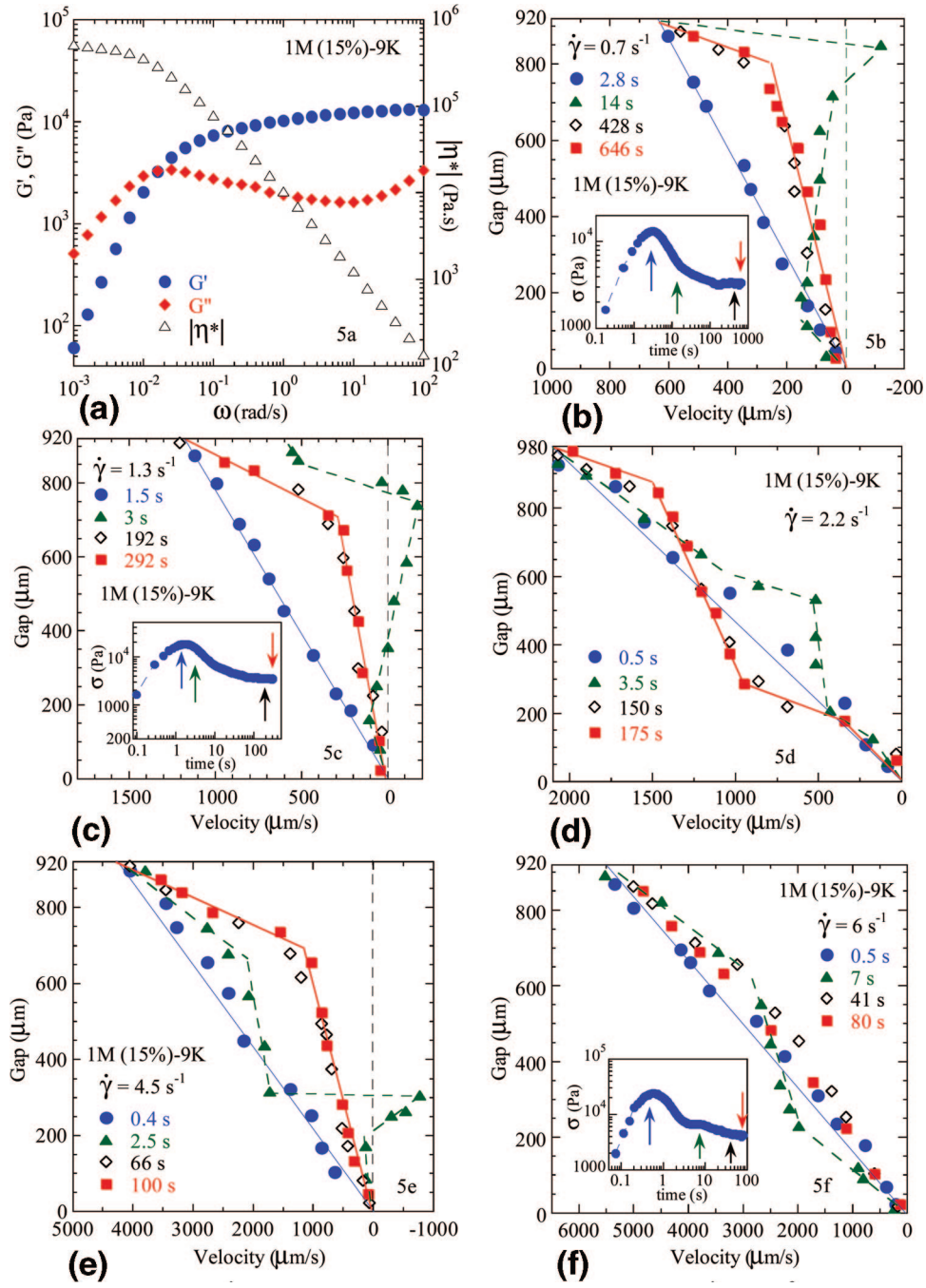

Figure 5. (a) Linear viscoelastic measurements of 1M (15%)-9K solution at room temperature. (b−e) Velocity profiles at different times for shear rates mentioned in the figures. Corresponding rheological data have been shown in the inset for some of them. A 25 mm parallel disk was employed on a Bohlin-CVOR rheometer. (f) Restoration of near linear velocity profile at a sufficiently high applied rate.

entropic barrier preventing the sample from attaining uniform disentanglement. We have recently shown that there is an entropy loss on the order of k_BT for disappearance of each entanglement point.[40] In other words, breakdown of cohesion of the entanglement network requires supply of energy. It is also possible to show that inhomogeneous dissolution of chain entanglement involves a smaller loss of chain entanglement than homogeneous removal of entanglement. Thus, once the sample breaks up inhomogeneously initially, it can avoid losing more entanglement points by remaining in a state of inhomogeneous shear. If a balance is established between the viscous dissipation and the external rate of work, there may not be additional energy available to remove more chain entanglements, and consequently the system may get stuck in a permanent state of inhomogeneity. This appears to be the case as witnessed by our PTV observations presented in Figure 3c−f.

B. Homogeneous Shear upon Sufficient Disentanglement at High Rates. It is important to note that at a high applied rate of $\dot{\gamma}_h \sim 6\ s^{-1}$ the sample shows a tendency to return to homogeneous shear, as seen in Figure 3h. We can estimate the level of remaining chain entanglement at $\dot{\gamma}_h$ by assuming that the zero-shear viscosity $\eta_0 \sim NZ^{2.4}$ and $\eta_h = \eta_0/(\dot{\gamma}_h\tau) \sim NZ_h^{2.4}$, so that $Z_h = Z/(\dot{\gamma}_h\tau)^{1/2.4} \sim 5$.

C. 1.8M (10%)-9K, 1M (15%)-9K, and 1.8M (15%)-15K Solutions (Z > 40). To further increase the chain entanglement, we studied 1.8M (10%)-9K solution with $Z = 70$. Oscillatory shear frequency sweep measurements shown in Figure 4a clearly indicates a level of polydispersity. The transient and steady-

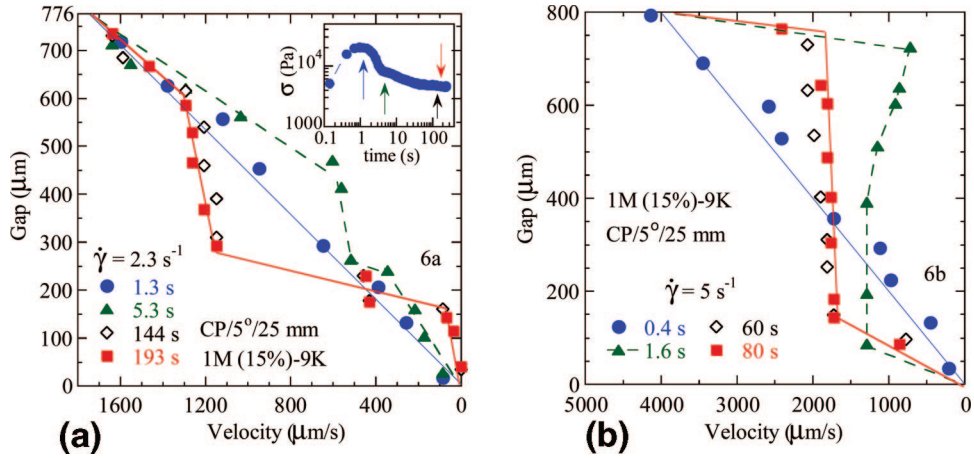

Figure 6. (a, b) Velocity profiles at different times for shear rates mentioned in the figures. Cone−plate of 25 mm diameter and 5° were employed on a Bohlin-CVOR rheometer.

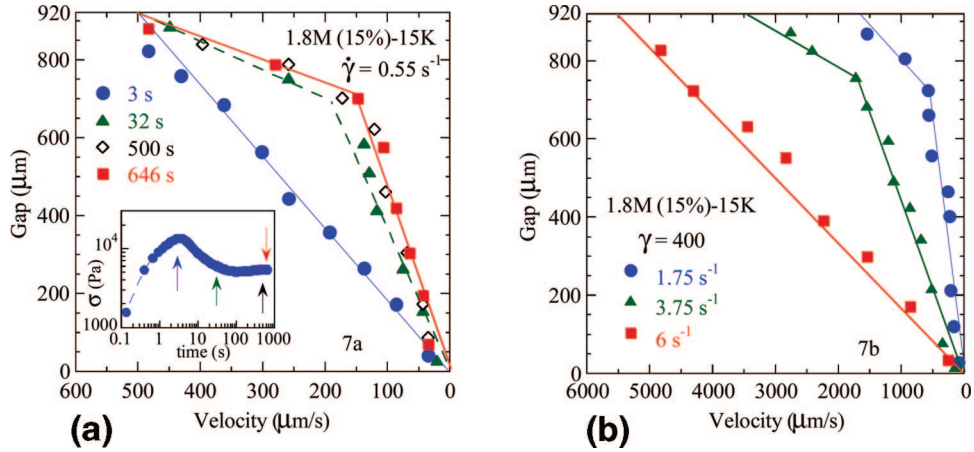

Figure 7. (a) Velocity profiles of 0.55 s^{-1} at different times measured on a Bohlin rheometer using a 25 mm parallel disk for the 1.8M (15%)-15K solution. (b) Velocity profiles at 400 strain units are summarized for the various rates mentioned in the figure.

state flow profiles at a rate of 1.5 s^{-1} shown in Figure 4b are similar to profiles of 1M (10%)-9K solution reported in Figure 3c−f. After the initial inhomogeneous failure of the entanglement network, the sample settles to a steady banding profile represented by open triangle, open diamond, and closed square symbols. As seen from Figure 4b, there is hardly any change in the flow profile between 166 and 253 s, during which 130 strain units elapse. The local shear rate in the fast shear band is 10 times higher than that in the low-shear band. Figure 4c summarizes the velocity profiles in steady state at various apparent shear rates. For the apparent shear rates of 2.5, 4, and 6.5 s^{-1}, the local rate in the high-shear band is also around 10 times faster than that in the low-shear band.

Our other solution of $Z = 64$ involves a concentration of 15 wt % PBD of M_w equal to 1 million g/mol. Owing to the increased concentration, 25 mm disks had to be used to prevent torque overloading, and PTV observations were made 4 mm away from the edge. Linear viscoelastic measurements are presented in Figure 5a. Figure 5b−f shows the profiles at different times for apparent rates of 0.7, 1.3, 2.2, 4.5, and 6.0 s^{-1}, respectively, at the PTV observation plane. From Figure 5b to 5e, it can be seen that inhomogeneity happens by occurrence of elastic recoil-like motions within the bulk of the sample. Figure 5d involves a separate sample loading and shows a different profile similar to those obtained with cone−plate cell as depicted below. Figure 5f is analogous to Figure 3h, where nearly uniform shear is restored. For the same sample, we have also conducted PTV observations using a cone−plate cell of 25 mm diameter and 5.4° cone angle. Parts a and b of Figure 6 indicate shear banding at the different stages for two applied rates of 2.3 and 5 s^{-1}, respectively. Figure 7a shows the velocity profiles at 0.55 s^{-1} for 1.8M (15%)-15K solution with $Z = 119$ in a 25 mm parallel disk. The steady-state profiles at various rates have been summarized in Figure 7b.

4. Summary

Six entangled polybutadiene solutions of varying number of entanglements per chain from $Z = 13$ to 119 have been subjected to various apparent rates of simple shear in standard rotational rheometry to explore their nonlinear flow behavior in terms of the corresponding velocity profiles. Our particle tracking velocimetric technique allows us to examine whether a sample would undergo homogeneous shear in absence of any measurable wall slip that can be suppressed by using polymeric solvents. It is found that the least entangled solution with $Z = 13$ exhibited homogeneous shear at all times. The solution with $Z = 27$ transiently developed shear banding after the shear stress maximum before returning to shear homogeneity in steady state. For solutions with $Z \geq 40$, shear inhomogeneity emerges after stress overshoot. Far beyond the terminal flow region, coexistence of low- and high-shear-rate states survives even after hundreds of strain units of shearing, indicating that different states of chain entanglement are possible corresponding to the same shear stress. At sufficiently high rates, the velocity profile approximately recovers linearity in steady state, where entangled solutions may become sufficiently disentangled. The present collection of PTV observations systematically examined how

shear inhomogeneity occurs and when linear velocity variation reemerges as a function of the level of chain entanglement and the intensity of the imposed shear flow.

Observations of shear banding in well-entangled polymers are unexpected according to the traditional perception that a liquid is a liquid no matter how viscoelastic it is. Actually, it is not difficult to perceive a well-entangled polymer to suffer inhomogeneous shear in response to large external deformation that is taking place much faster than the chainlike molecules have the time (i.e., terminal relaxation time τ) to move around. On a time scale far shorter than τ, an entangled polymer could simply undergo cohesive breakdown if the imposed external deformation is arbitrarily high. During its solidlike response, any local structural failure could immediately allow other layers of the sample to avoid disintegration in the case of simple shear. This is the origin of temporary shear inhomogeneity. A second traditional perception tells us that at long times (far exceeding τ) when even a strongly viscoelastic entangled polymer can be regarded as a liquid the steady state of shear should be spatially homogeneous and independent of the prior flow history and independent of the mode (controlled force vs controlled displacement) used to generate shear steady shear. Here, it is indeed surprising that shear banding would prevail in steady state. We are merely at the beginning of confirming such permanent banding in entangled polymer solutions and developing a phenomenological understanding of why shear banding is stable.

Acknowledgment. This work is supported, in part, by a small grant for exploratory research from National Science Foundation (DMR 0603951) and by a PRF grant from American Chemical Society (#40596-AC7).

Note Added After ASAP Publication. This article was published ASAP on March 8, 2008. Two text changes have been made in paragraph 3.3 (B) of the Results and Discussion section. The correct version was published on April 1, 2008.

References and Notes

(1) Huppler, J. D. *Trans. Soc. Rheol.* **1967**, *11*, 181.
(2) Lee, C. L.; Polmanteer, K. E.; King, E. G. *J. Polym. Sci., Part A-2* **1970**, *8*, 1909.
(3) Graessley, W. W. *Adv. Polym. Sci.* **1974**, *16*, 1.
(4) Osaki, K.; Fukuda, M.; Ohta, S. I.; Kim, B. S.; Kurata, M. *J. Polym. Sci., Polym. Phys. Ed.* **1975**, *13*, 1577.
(5) Graessley, W. W.; Park, W. S.; Crawley, R. L. *Rheol. Acta* **1977**, *16*, 291.
(6) Menezes, E. V.; Graessley, W. W. *J. Polym. Sci., Polym. Phys. Ed.* **1982**, *20*, 1817.
(7) Osaki, K.; Inoue, T.; Isomura, T. *J. Polym. Sci., Polym. Phys. Ed.* **2000**, *38*, 1917.
(8) Osaki, K.; Inoue, T.; Isomura, T. *J. Polym. Sci., Polym. Phys. Ed.* **2000**, *38*, 2043.
(9) Bercea, M.; Peiti, C.; Simionescu, B.; Navard, P. *Macromolecules* **1993**, *26*, 7095.
(10) Mhetar, V. R.; Archer, L. A. *J. Polym. Sci., Polym. Phys. Ed.* **2000**, *38*, 222.
(11) Pattamaprom, C.; Larson, R. G. *Macromolecules* **2001**, *34*, 5229.
(12) Islam, M. T.; Archer, L. A. *J. Polym. Sci., Polym. Phys. Ed.* **2001**, *39*, 2275.
(13) Rehage, H.; Hoffmann, H. *J. Phys. Chem.* **1988**, *92*, 4712.
(14) Rehage, H.; Hoffmann, H. *Mol. Phys.* **1991**, *74*, 933.
(15) Callaghan, P. T.; et al. *J. Phys. II* **1996**, *6*, 375.
(16) Mair, R. W.; Callaghan, P. T. *Europhys. Lett.* **1996**, *36*, 719.
(17) Britton, M. M.; Callaghan, P. T. *Phys. Rev. Lett.* **199730**, 4930.
(18) Britton, M. M.; Mair, R. W.; Lambert, R. K.; Callaghan, P. T. *J. Rheol.* **1999**, *43*, 897.
(19) Fischer, E.; Callaghan, P. T. *Europhys. Lett.* **2000**, *50*, 803.
(20) Salmon, J. B.; Colin, A.; Manneville, S.; Molino, F. *Phys. Rev. Lett.* **2003**, *90*, 228303.
(21) Salmon, J. B.; Manneville, S.; Colin, A. *Phys. Rev. E* **2003**, *68*, 051503.
(22) Becu, L.; Manneville, S.; Colin, A. *Phys. Rev. Lett.* **2004**, *93*, 018301.
(23) Hu, Y. T.; Lips, A. *J. Rheol.* **2005**, *49*, 1001.
(24) Lopez-Gonzalez, M. R.; Holmes, W. M.; Callaghan, P. T. *Soft Matter* **2006**, *2*, 855.
(25) Tapadia, P.; Wang, S. Q. *Phys. Rev. Lett.* **2006**, *96*, 016001. . In contrast to the other available methods capable of determining velocity profiles, such as NMR imaging and ultrasound spectroscopy that are both indirect and have poor time resolution, a particle tracking velocimetric technique was employed in this study to allow simultaneous determination of conventional rheometric measurements and in-situ observation of the actual flow field generated in a standard rotational rheometer.
(26) Boukany, P. E.; Wang, S. Q. *J. Rheol.* **2007**, *51*, 217.
(27) (a) Lu, C. Y. D.; Olmsted, P. D.; Ball, R. C. *Phys. Rev. Lett.* **2000**, *84*, 642. (b) Fielding, S. M.; Olmsted, P. D. *Phys. Rev. Lett.* **2004**, *92*, 084502.
(28) Vasquez, P. A.; McKinley, G. H.; Cook, L. P. *J. Non-Newtonian Fluid Mech.* **2007**, *144*, 122.
(29) Bautista, F.; Soltero, J. F. A.; Perez-Lopez, J. H.; Puig, J. E.; Manero, O. *J. Non-Newtonian Fluid Mech.* **2000**, *94*, 57.
(30) Doi, M.; Edwards, S. F. *The Theory of Polymer Dynamics*; Clarendon Press: Oxford, 1986.
(31) Cates, M. E.; McLeish, T. C. B.; Marrucci, G. *Europhys. Lett.* **1993**, *21*, 451.
(32) Marrucci, G. *J. Non-Newtonian Fluid Mech.* **1996**, *62*, 279.
(33) Milner, S. T.; McLeish, T. C. B.; Likhtman, A. E. *J. Rheol.* **2001**, *45*, 539.
(34) Graham, R. S.; Likhtman, A. E.; McLeish, T. C. B.; Milner, S. T. *J. Rheol.* **2003**, *47*, 1171.
(35) Doi, M.; Edwards, S. F. *J. Chem. Soc., Faraday Trans. 2* **1979**, *75*, 38.
(36) Wang, S. Q. *Phys. Rev. Lett.* **2006**, *97*, 187801.
(37) Ravindranath, S.; Wang, S. Q. *Macromolecules* **2007**, *40*, 8031.
(38) Hu, Y. T.; Wilen, L.; Philips, A.; Lips, A. *J. Rheol.* **2007**, *51*, 275.
(39) Wang, S.; Wang, S. Q.; Halasa, A.; Hsu, W. L. *Macromolecules* **2003**, *36*, 5355.
(40) Wang, S. Q.; Ravindranath, S.; Wang, Y.; Boukany, P. *J. Chem. Phys.* **2007**, *127*, 064903.

MA7027352